Aeroacoustics Conferences
May 27-29, 2013, Berlin, Germany
19th AIAA/CEAS Aeroacoustics Conference

Direct flow-induced noise prediction of a simplified HVAC duct using a Lattice Boltzmann Method

Franck Pérot[1], Mohammed Meskine[2]
Exa Corporation, 150 North Hill Drive, Brisbane, CA, 94005, USA

Jörg Ocker[3]
Porsche AG, D-71286 Weissach, Germany

For the automotive industry, the quality and levels of airborne noise contributions from HVAC systems has a growing importance and has to be addressed as early as possible in the development process. Flow-induced noise is generated by the turbulent flow circulating in the ducted system and by the vents flows. Flow detachments and separations, strong turbulent interaction and mixing and duct resonances are typical mechanisms related to the production of the flow-induced noise contribution. Previous studies have demonstrated the accuracy of simulations based on Lattice Boltzmann Method at capturing simultaneously transient flows and their noise contributions induced by production automotive HVAC face ducts, vents, mixing units and blowers as well as complete HVAC systems. Some validation studies on simplified configurations have also been proposed. In this paper, our attention is focused on another simplified geometry used as a validation benchmark case by a German car manufacturer's aeroacoustics consortium. Even if the configuration discussed in this work is geometrically relatively simple, complex and sensitive flow mechanisms and very low radiated noise levels compare to real configuration are involved. As a consequence, such a configuration represents a challenging test case for CFD/CAA solutions.

I. Introduction

Cabin acoustic comfort has a growing importance for the automotive industry. Considering the significant reduction of other traditional sources, the contribution of HVAC systems is now to be considered as early as possible in the vehicle development process. At high flow rates and in the frequency range from about 200 Hz to 3000 Hz, aerodynamics noise produced by unsteady flow fluctuations, propagating inside the ducted system and radiating into the cabin is likely to be one of the most important noise contribution[1]. The use of CFD/CAA prediction solutions is in rapid expansion representing an alternative to time-consuming and expensive prototyping[2] and offering a valuable diagnosis tool to visualize and understand better the noise generation mechanisms and locations. In addition, such an approach represents an efficient way to reduce, and eventually optimize, the noise produced by HVAC systems[2]. Previous published studies on simplified ducts[4], production face ducts and vents[1,4-6], mixing units[7], blowers[8,9] and complete HVAC systems[3,10] have shown the possibility to use LBM simulations as an engineering design solution. This type of simulation also represents an interesting diagnostic tool helping at identifying the location of flow-induced noise sources[3].

In the present study, CFD/CAA calculations are performed on a simplified duct configuration and compared to experimental results. This configuration, an elbow duct containing a flap, is experimentally characterized and used as a validation test case in the context of a German car manufacturer's aeroacoustics consortium. Some flow measurements using Particle Image Velocimetry (PIV), Wall Pressure fluctuations (WPF) and radiated acoustics measurements are performed out in an anechoic room. The PIV and WPF results are reported by Jager et *al*.[11]. Even if this configuration is relatively simple, some complex and sensitive mechanisms are involved.

[1] Director, Aeroacoustics Applications, perot@exa.com, AIAA Member
[2] Principal aeroacoustics engineer, Aeroacoustics Applications, mmeskine@exa.com
[3] Dr.-Ing. h.c.F., joerg.ocker@porsche.de

Simulations are carried out using a transient, explicit and compressible CFD/CAA solver based on the resolution of the discretized Boltzmann equation known as Lattice Boltzmann Method (LBM). The LBM-based PowerFLOW CFD/CAA solver is used to predict simultaneously unsteady flow mechanisms and the corresponding flow-induced noise contributions. Unlike two-steps procedure based on acoustics analogies and requiring the coupling between aerodynamics information to an acoustic propagation solver[14-15], in this study the noise is predicted in one-step during the CFD/CAA simulations. Previous studies have shown the potential of this method at propagating acoustics waves[12,13] and accurately predict the flow-induced noise contribution from HVAC systems[1-10]. This method presents a net interest in terms of accuracy, process simplicity and turnaround times.
Some details on the measurements are briefly described in a first section. In the second and third sections, information on numerical method is given and the simulation results compared to experiments and the effects of the inlet velocity profile are discussed. In the last part, the pseudo-noise contribution measured at the far-field microphones is filtered out from the predicted results by using an acoustic analogy method.

II. Experimental Setup

As shown in Figure 1a, the 90° bended duct has a rectangular cross section (80x80 mm^2) and contains an obstacle taking the shape of a simplified throttle flap. For PIV measurements, the duct is made with transparent acrylic glass and with aluminum for the acoustics measurements. The flow is driven with a variable speed fan causing fundamental fan harmonics related to the Blade Passing Frequency and harmonics above 1000 Hz. Two mufflers in a tandem configuration are inserted into the system to damp this spurious fan noise contribution (Figure 1b). An adapter insures a smooth transition from the circular cross section of the mufflers to a quadratic cross section (80x80 mm^2). At the downstream end of the adaptor a 1.5mm tripping ridge is installed at the circumference of the duct to force the development of a turbulent boundary layer. The boundary layer develops over a 3 m distance and a fully turbulent flow is expected to be present at the inlet of the elbow duct.
Unsteady wall pressure fluctuations are measured at seven positions at the surface of the duct using wall flush mounted ¼ inch microphones. The locations of the seven microphones are depicted in Figure 2. PIV measurements are conducted inside the duct providing mean flow information.

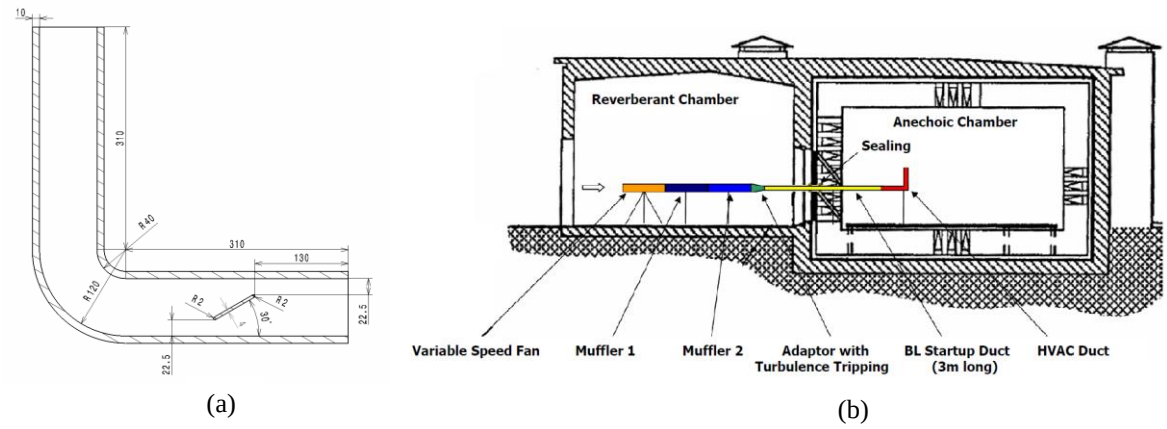

(a) (b)

Figure 1. (a) Duct schematic representation; (b) Experimental setup and facility

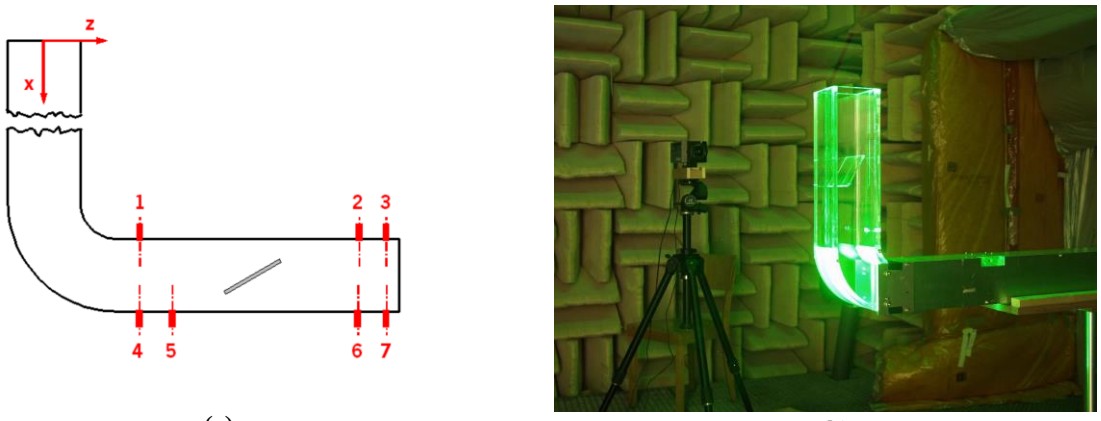

(a) (b)

Figure 2. (a) Wall Pressure Fluctuations measurement locations; (b) PIV experimental setup.

The radiated noise is measured at 17 microphones positioned on a semi-circular antenna (Figure 3a and 3b). The angle of the antenna is varied in such a way the noise is measured at 17 angular positions. These measurements provide a complete characterization of the directivity on a hemisphere composed by 17x17=289 points and the averaged Sound Pressure Levels (SPL), proportional to the radiated acoustic power L_w, is estimated by averaging the 289 Sound Pressure Levels (SPL).

Some of the microphones are directly impacted by the jet coming out of the duct. This phenomenon is responsible for an increase of the noise levels related to the pseudo noise contribution (convective mechanisms). A spatial filtering operation is applied to these microphones to filter out this contribution and extract, as precisely as possible, the pure noise contribution from the signals. The exact procedure used to process the experimental signals is not exactly known by the authors and another method based on an acoustic analogy is used in Section IV.

Measured SPLs are shown in Figure 4. The red plot represents the averaged SPL and the gray ones correspond to the minimum and maximum SPL. A significant directivity effect is observed with a difference by 10-15 dB between the lower and higher measured SPL. The lower levels are measured in a perpendicular direction to the mean flow direction at the exit whereas the higher levels are measured in the axis of the jet.

In comparison to usual HVAC measurements, the noise levels are presently relatively low (20-30dB) in the frequency range from 50 to 200Hz, dropping to 0-10 dB at higher frequencies. The maximum frequency of interest is then limited to about 1000 Hz. Very low frequency noise (f <50-100Hz) can be affected by the background noise of the facility and are barely exploitable. The origin of the peaks remained unclear and might be related to duct modes excited by the turbulent flow or to periodic vortex shedding occurring in the system. This point is discussed in detail in the numerical part by analyzing the transient flow results.

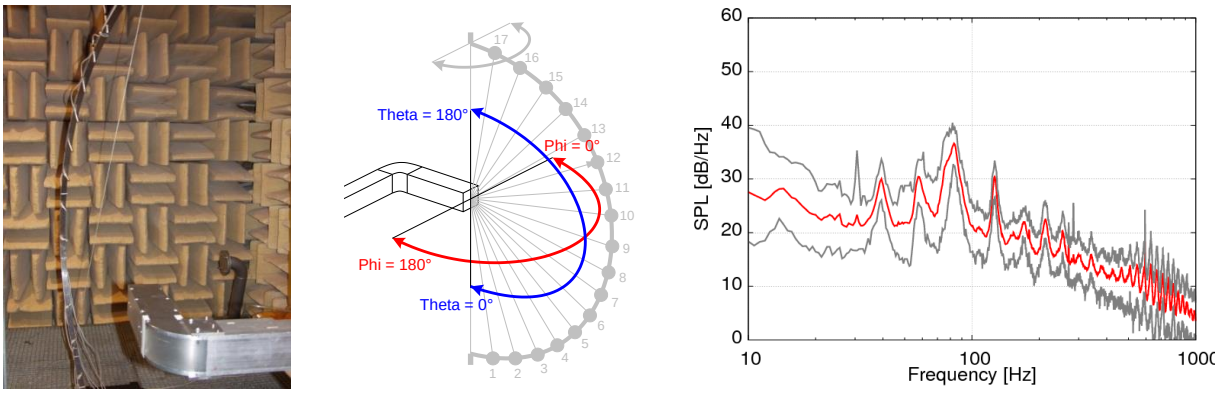

(a) (b) (c)

Figure 3. (a) Acoustics antenna; (b) Microphone locations and antenna rotation property; (c) Radiated noise levels: (——) average SPL, (——) minimum and maximum SPL, pseudo noise contribution removed.

III. Numerical Setup

A. Lattice Boltzmann Method

The CFD/CAA solver PowerFLOW based on the Lattice Boltzmann Method (LBM) is used to calculate unsteady flow physics and the corresponding flow-induced noise generation and radiation. Lattice-based methods are by nature explicit, transient and compressible, and are an alternative to traditional CFD methods based on the discretization of the Navier-Stokes equations and derived variations. The basic idea of LBM is to track the advection and collisions of fluid particles. Since the average number of particles in a representative volume of fluid far exceeds the compute power required to track them individually, the particles are grouped into an integer number of discrete directions with index *i*. The computation follows the particle distribution function f_i which represents the number of particles per unit of volume, also called voxel, at a specific time and location moving with velocity c_i. As in statistical physics, the flow variables such as density and velocity are determined by taking the appropriate moments, *i.e.* summations over the set of discrete directions, of the particle distribution function. LBM is used and validated across many aeroacoustics applications such as automotive wind-noise[16,17], sunroof buffeting[18], , acoustics propagation[12,19,20], fan noise[21-23,], airframe noise[24], etc…Additional theoretical details on LBM can be found in the cited references[25-29].

B. Far-field noise calculation

Although LBM has intrinsic CAA capabilities and computes the noise directly from unsteady flow simulations, an integral extrapolation method based on an acoustic analogy has been developed. This method is usually used when the distance between the sources and the microphones is prohibitively large and cannot be covered by the CFD computational domain. An integral solver based on the forward-time resolution of the FW-H equation based on Farassat's formulation 1a can then used[19]. Details about the formulation are given in[20-22]. The FW-H solver is embedded in the post-processing software PowerACOUSTICS used to perform any statistical and spectral analyses of the transient information generated by PowerFLOW. The post-processing can be run in batch mode, allowing a full automation of the digital procedure.

Two formulations are implemented in the FW-H solver[20]:

- Permeable-surface (also called "porous" FW-H formulation). Pressure, density and the three velocity components recorded at a fictive surface are used.
- Solid formulation. Only the pressure fluctuation on solid surfaces, corresponding to physical surfaces, is used.

To take into account for ground reflections, an image method including the possibility to assign a specific absorption coefficient is used. The far-field noise is calculated either using a wind-tunnel formulation or a pass-by (or fly-over) formulation including Doppler effects.

In section IV, the porous formulation in wind-tunnel mode is used. The noise at the far-field microphones is actually predicted directly with LBM and the usage of FW-H is not needed to generate accurate radiated noise results. However, similarly to experiments performed without windshields on the microphones, the predicted signals from LBM might contain a pseudo-noise contribution corresponding, for instance and for the present case, to the impact of the outlet jet flow. Since the pseudo-noise contribution has been filtered out from the experiments, the same procedure has to be applied to the simulated results. By definition the output signals from FW-H are purely acoustics signals and this method can present a simple way to filter out the pseudo-noise from the directly simulated pressure signals. The main questions related to this approach are related to the correct inclusion of diffraction effects from the duct and the effect of convective mechanisms crossing the porous surface. To investigate the first point, a pure acoustics test case is discussed in Section IV. For the second point, investigations on the tandem cylinders[30] or train configurations[31-32] provide an *a priori* confidence in the method.

C. LBM Simulation details

The simulated elbow duct geometry is embedded into a large cubical simulation domain. The floor is modeled as a wall and the six outlets faces corresponding to the boundary of the simulation domain are defined as pressure outlets. Some acoustic sponge zones are included in the simulation domain to avoid spurious reflections from the boundary conditions and model a digital semi-anechoic chamber similar to an experimental one. In the whole domain, the initial pressure is set to the atmospheric pressure p_0=101325 Pa and the initial velocity is set to zero. The boundary condition at the inlet of the duct is a velocity inlet. Similarly to the experiments, the inlet duct contains an anechoic termination modeled with a sponge zone avoiding most of the reflections from acoustics waves generated in the system and propagating downstream in direction of the inlet boundary condition.

Two different inlet velocity profiles are imposed. The first one corresponds to the inlet velocity profile measured with PIV and the second one to a uniform inlet velocity profile. For both inlet conditions, the averaged flow speeds is U~7.5 m/s and have both the same mass flow. Two simulations are presented in this paper, simulation A using a uniform inlet velocity profile and simulation B using the experimental one. The first goal of this study is to check the sensitivity of the results to the inlet boundary conditions and particularly to the impact of the near wall velocity gradients on the bend detachment. The second goal is to check if a measured 2-D profile is sufficient to precisely characterize the 3-D inlet boundary condition of the simulations. This investigation will provide an estimation of the impact and importance of this parameter on the results having a physical meaning on the measured quantities.

A generic and fully automated resolution scheme is developed and was used in previous published studies. A grid resolution showing the convergence of the results with respect to the spatial discretization has been performed but the results are not presented in this paper. The final mesh grid is shown in Figure 4. The finest cell size is applied around the flap and the second mesh level, twice coarser, is applied inside the duct and at the exit. The grid cell size is progressively increased going outward from the duct exit and controlled using spheres centred on the outlet. From one sphere to another, as seen in Figure 4, the grid cell size varies by a factor of two. The simulated physical time is 0.7s.

The radiated acoustic pressure fluctuations obtained directly from the transient flow simulation are recorded at 289 locations (probes) corresponding to the experiments. From those pressure time histories, SPL are calculated and the average SPL calculated the same way as the experiments.

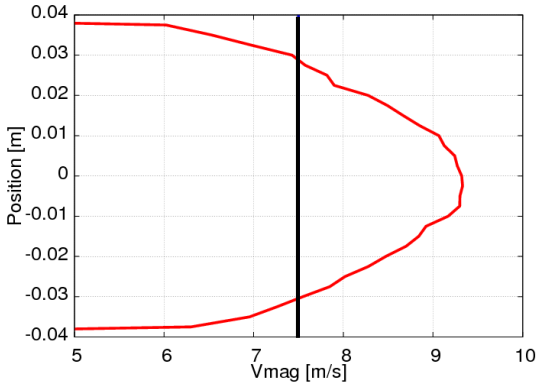

Figure 4. Mean inlet velocity at the duct inlet. (—) experiments and simulation B, (—) simulation A.

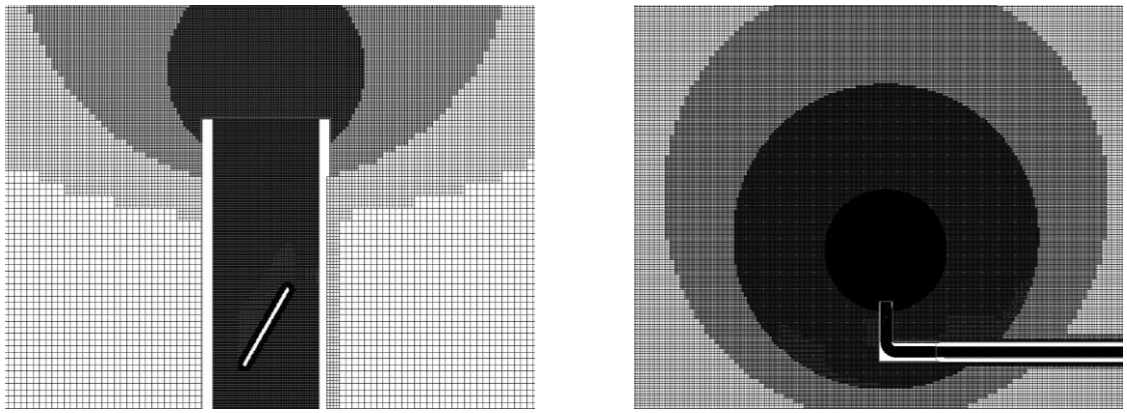

Figure 5. LBM spatial grid represented in a *y*-plane.

IV. Flow and Noise Results

A. Mean flow analysis

The velocity vectors obtained from the PIV measurements and the simulations A and B are represented in Figure 6. The comparison is very satisfying both in term of mean flow topology and absolute velocity values. These results highlight the presence of six main regions:

1. Attached flow development on the opposite side to the bend,
2. Flow separation occurs at the bend driven by the adverse pressure gradient,
3. Shear layer induced by the separation at the bend interacting with the flap,
4. Recirculating zone in the wake of the flap,
5. Strong flow acceleration and mixing on the upper and lower regions of the flap,
6. Jet development (shown in Figure 7).

The main difference between simulations A and B is related to the position and the intensity of the shear layer developing from the flow separation in region 2. Using the experimental velocity profile (simulation B), the separation angle is bigger compare to simulation A impacting the bottom area of the flap. Considering the shape of the experimental profile, the near-wall velocities upstream the flow separation for simulation B are smaller than simulation A. As a consequence, the adverse pressure gradient in the detachment area is bigger for simulation A, keeping the flow more attached. It can also be noticed that for simulation B the flow velocity are higher right below the flap and that the flow velocities at the exit is smaller. The boundary layer and the near-wall flow at the duct exit are then affected by the inlet velocity profile.

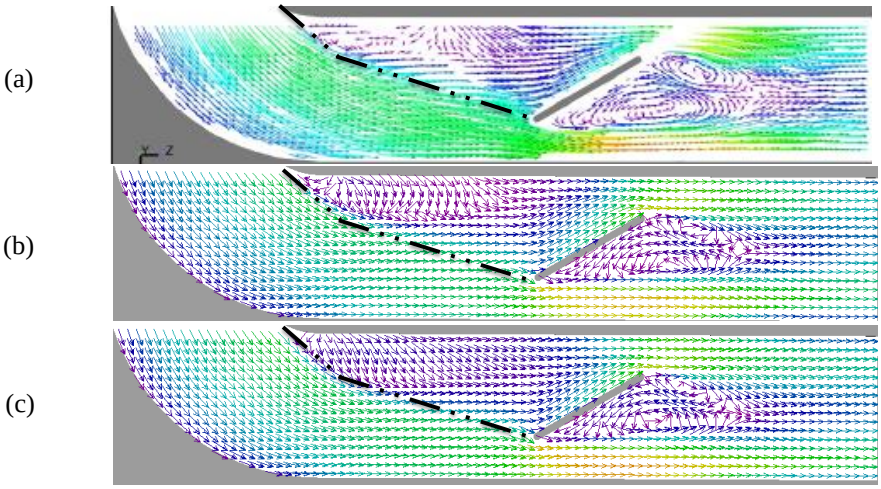

Figure 6. Mean velocity vectors in the center plane of the duct: (a) PIV; (b) simulation A; (c) simulation B.

B. Unsteady flow analysis

The instantaneous velocity and vorticity fields are plotted in Figure 7 and highlight more clearly the six regions described in the previous section. In particular, little turbulent activity occurs in region 1 and the velocity levels and the flow unsteadiness is stronger in regions 3 and 5. Time animations show the presence of coherent flow structures in the different shear layers and a flapping mechanism is clearly noticeable in the wake of the flap. This flapping, stronger for configuration A, seems similar to a Kármán shedding mechanism occurring in the wake of a circular cylinder. Under this hypothesis and assuming a constant Strouhal number $S=d \cdot f_0/U_0$ ~0.2 with d and U_0 some characteristic dimension and velocity of the problem, respectively, the value of a possible shedding frequency f_0 in the system is given by $f_0=S \cdot U_0/d$. Taking d as the projected length of the flap and U_0~10-12m/s (from Figure 6 results), the shedding frequency would be in the range 70 Hz < f_0 < 90 Hz. This result is further discussing in the following sections. Another interesting result is that the wake of the flap and the possible shedding impacts more strongly the upper part of the duct near the exit in simulation B.

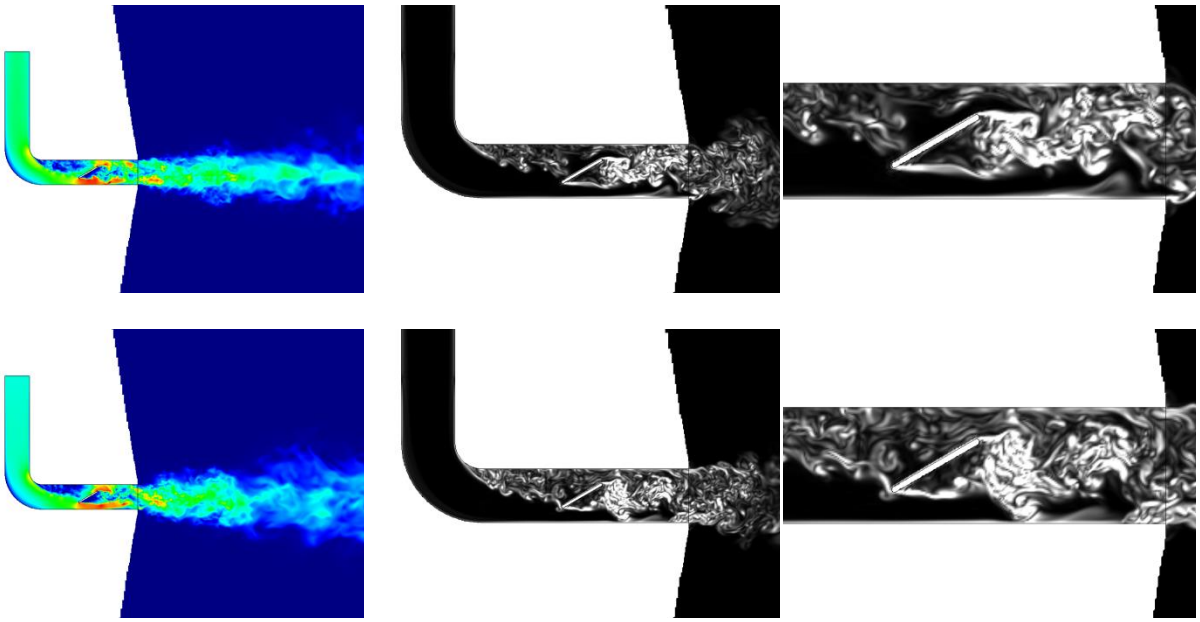

(a) (b) (c)

Figure 7. (a) Instantaneous velocity (b)-(c) instantaneous vorticity fields in a y-plane passing through the center of the duct fields. Top: Simulation A; Bottom: Simulation B.

C. Wall Pressure Fluctuations

Wall Pressure fluctuations at microphones 1 to 7 are plotted in Figure 8. A very satisfying agreement between measurements and the simulations is overall obtained, particularly for microphones 2, 3 and 6 and 7 corresponding to regions where the flow is strongly separated for which the broadband levels are the highest. At microphones 6 and 7, a significant improvement is obtained using the experimental profile (simulation B) for which the predictions above 100 Hz are in much better agreement with the experiments. This behaviour is likely related to the observation made in the previous section. With the experimental profile, it was indeed noticed that the wake of the flap and the shedding was impacting more strongly the lower part of the duct exit. Consequently, more flow structures in simulation B are present in this region explaining the increase of WPF levels corresponding (mainly) to the trace in pressure of convective mechanisms, *i.e.* coherent flow structures.

The results at microphones 4 and 5 are in good agreement with the measurements up to f~200-300 Hz. For higher frequencies, the simulations underestimate the experiments and a limited effect of the inlet profile is observed. In the lower part of the duct the flow was shown to be attached and consequently a turbulent boundary layer, likely not fully developed, exists. This underestimation is then certainly related to the fact that the spatial resolution used in the simulation is not sufficient to explicitly capture the tiny near-wall boundary layer structures responsible for the higher frequency contribution in the WPF.

The comparisons at microphone 1 are not satisfying above 100 Hz but this result is certainly interesting and provides an insight on the physical mechanisms. Indeed, both simulations overestimate the WPF levels which can be interpreted as the presence of more flow structures in the simulations compare to the experiments. In addition, the WPF results for simulation A are closer to the experiments. This behavior is in agreement with the previous observations related to the more intense flow separation occurring in simulation B. It can then be assumed that the location of the flow separation is slightly wrong compare to the experiments. An analysis of WPF in the proximity of probe 1 shows that the results are indeed sensitive to the location. To improve the present results, a better 3-D characterization of the inlet profile seems necessary.

Another interesting information contained in the WPF is the presence of a peak at 80 Hz on all microphones. In experiments, the second harmonics is also visible at microphones 2 and 3. This harmonics is likely present at the microphones 1, 4, 5, 6 and 7 but this phenomenon might be masked by the presence of high frequency mechanisms. The presence of this peak is captured in the simulations even if the levels are not perfectly predicted. Based on the analysis proposed in the previous section, the nature of this peak is related to a vortex shedding induced by the flap.

The effect of the inlet velocity profile in the instantaneous flow snapshots also offers an explanation to the observed trends. For instance, the peak levels are higher on the upper using the constant inlet profile because of the different direction of the wake and shedding (Figure 8). Some measurements carried out without the flap indicate that this 80 Hz mechanism is not present in the WPF SPL. This is another indication that this peak is related to a vortex shedding.

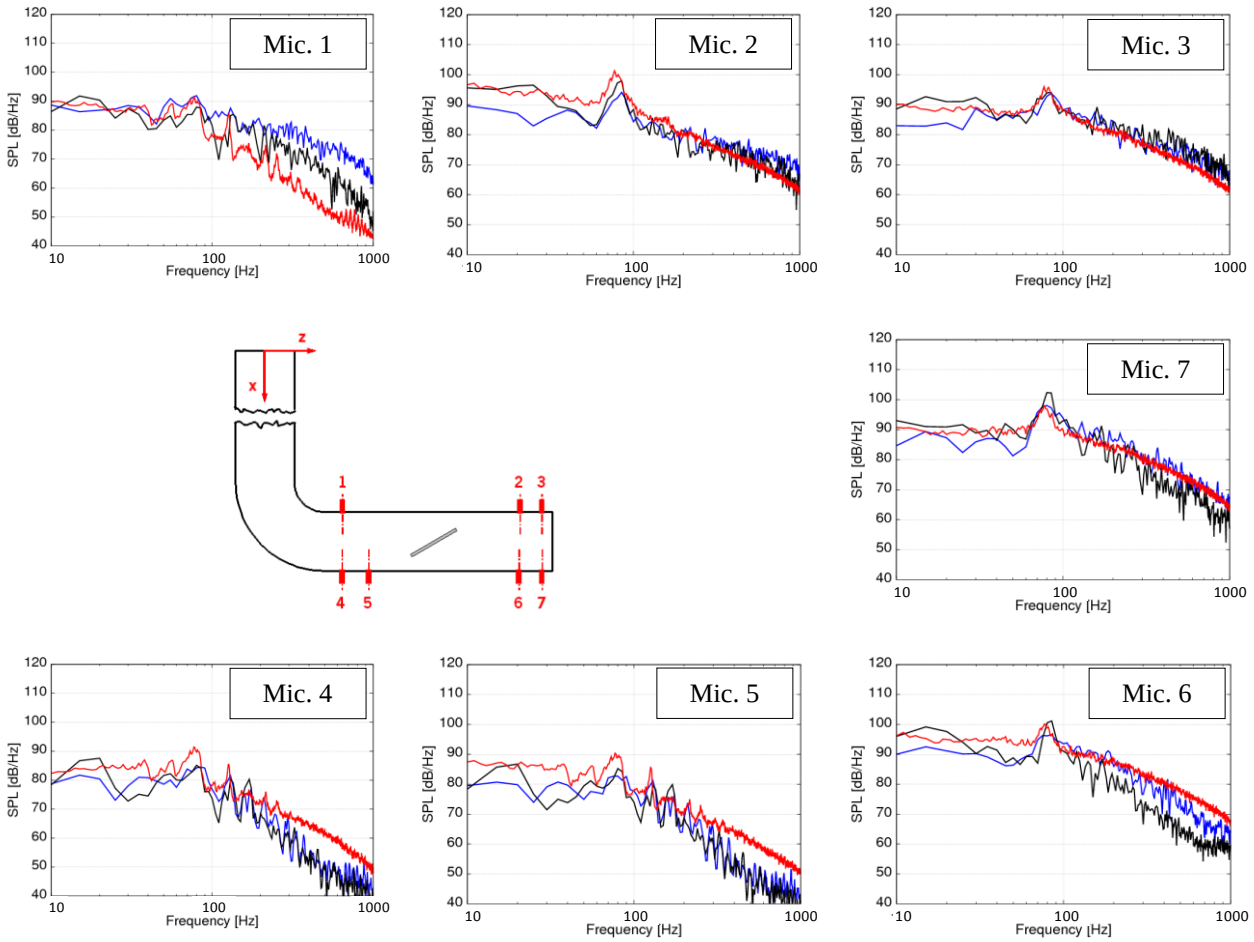

Figure 8. Wall Pressure Fluctuations. (—) experiments; (—) simulation A; (—) simulation B.

D. Fluid pressure fluctuations

Spectral analyses are performed on the instantaneous pressure information recorded in a *y*-plane. In the wake of the flap, the pressure dB-levels filtered around 80Hz highlight the presence of the intense fluctuations (Figure 9) indirectly confirming the presence of a coherent shedding mechanism previously mentioned. The main pressure fluctuations are located in the top region of the flap and are stronger for simulation B. This result is in qualitative agreement with the vorticity fields shown in Figure 5. For higher frequencies, the fluctuations are still more intense in the flap wake region but are visible in the whole domain and are spatially broadly spread. This is characteristic of flow-induced noise broadband sources.

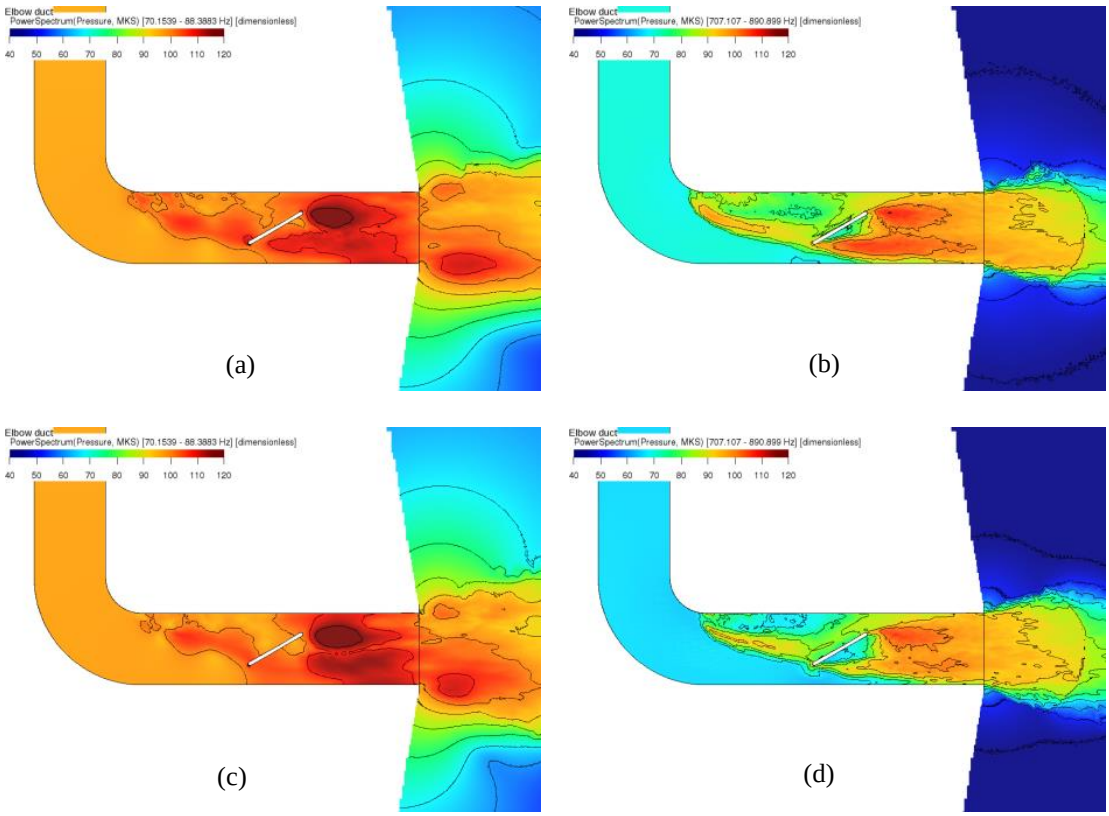

Figure 9. Fluid pressure fluctuations in decibels. (a)-(b) simulation A, (c)-(D) simulation B.

E. Radiated Noise

The averaged Sound Pressure Levels from simulations A and B are plotted in Figures 10. The predicted results are obtained directly with LBM at the same locations as the experiments. Simulations A and B provide very similar results above 100 Hz and for f>100 Hz, it can then be extrapolated that the inlet velocity profile does not drive the radiated noise results and implies that the main region responsible for the noise production is located in the wake of the flap. For f>100 Hz, the averaged predicted SPL overestimate the averaged measured SPL by 4-6 dB. The shape and slope of the results are similar and the predictions are visually shifted up. It is noticed that the averaged SPL are in very satisfying agreement with the maximum measured SPL. This point is addressed in the following section.

In the range 500-900Hz, many peaks are obtained both in experiments and with the simulation. The analysis of the transient flow results suggests that those peaks are related to shear layer instabilities.

Considering this low Mach number configuration, the contribution from the jet flow to the radiated noise levels is expected to be negligible and further investigations are ongoing to confirm this assumption.

Some acoustics measurements performed without the flap show noise levels about 20-30 dB lower. In addition the peak at 80 Hz and harmonics are still present even much lower as well. This interesting result could be explained by the fact that the noise radiated by the vortex shedding actually couples to acoustics duct modes. In case the flap is present, more energy is transferred to radiating duct modes enhancing their contributions to the radiated noise levels.

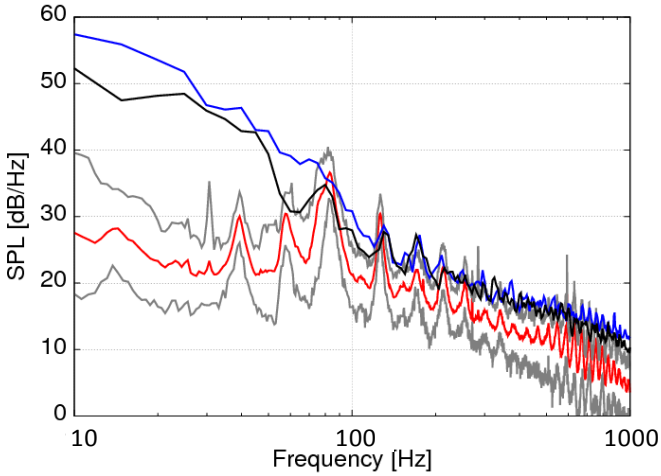

Figure 10. Averaged radiated SPL over the 289 microphones. (—) experiments; (—) minimum and maximum measured SPL; (—) simulation A; (—) simulation B.

Sound pressure levels at four positions A, B, C and D (Figure 11) are plotted in Figure 12. The influence of the inlet velocity profile on the radiated noise is confirmed to be negligible except maybe at low frequencies (f<80-100 Hz). Considering the previous transient flow analysis, this difference might be related to the flow separation and the corresponding shear layer interacting differently with the flap depending on the inlet profile.

The sound pressure levels at four positions confirm the overestimation noise close to the jet. Overall, the broadband content is in good agreement with the measurements and the shape of the SPL accurately captured. The predicted SPL overestimate by 2-3 dB the measurements above 100Hz and this overestimation is less pronounced compare to the averaged SPL in Figure 10. At microphone D, located in the jet region, the broadband levels above 300 Hz are in even better agreement with the measurements compare to microphones A, B and C. A strong overestimation below 300 Hz is obtained and is related to the pseudo-noise contribution which is filtered out from the measurements.

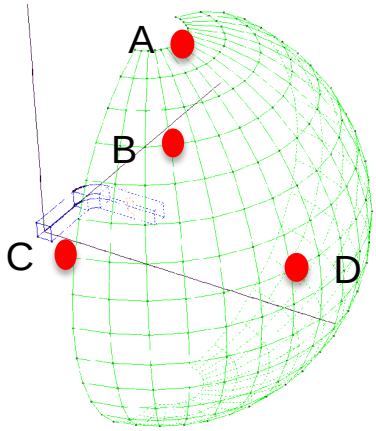

Figure 11. Position of microphones A, B, C and D.

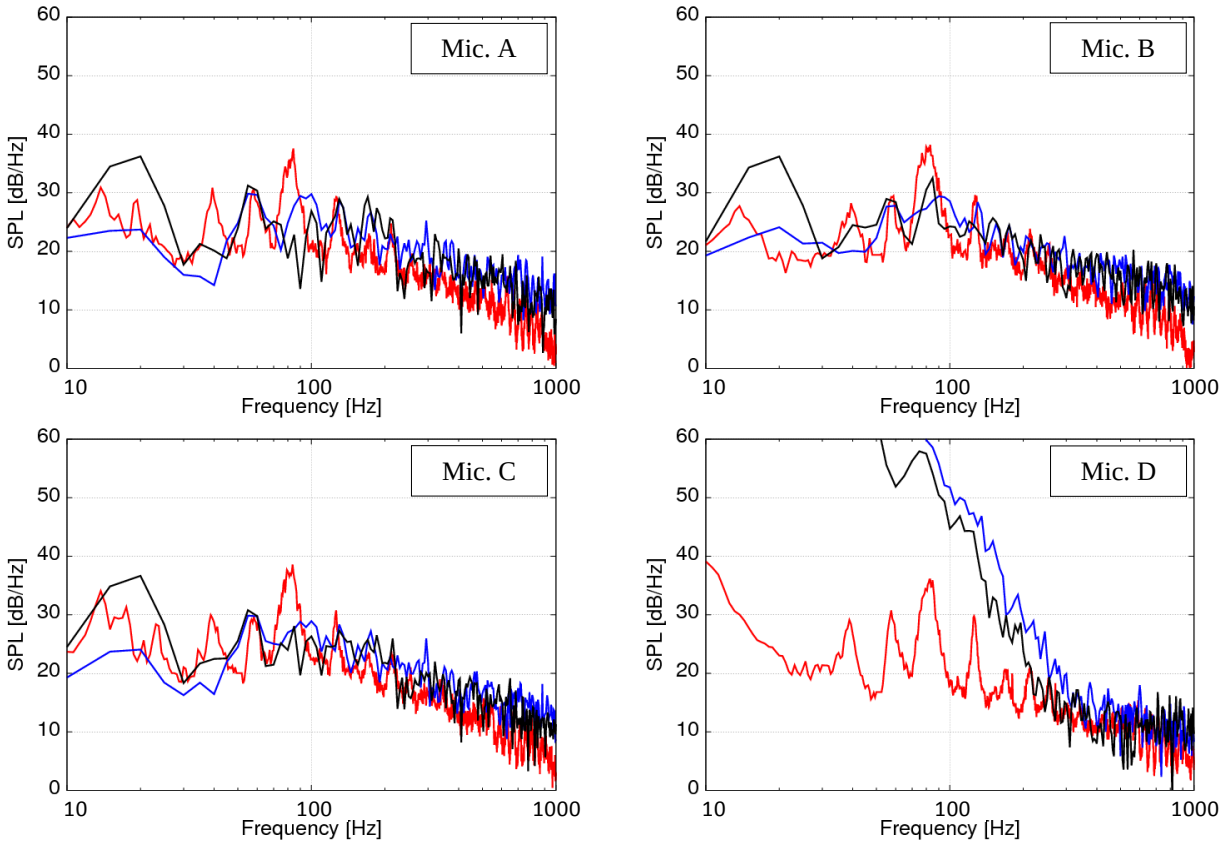

Figure 12. SPL at microphones A, B, C and D: (——) experiments; (——) simulation A; (——) simulation B.

F. Pseudo-noise contribution

The transient LBM results are recorded on a sample surface surrounding the duct outlet (Figure 13) and coupled to a porous FW-H acoustic analogy solver presented in Section III-b. To validate the far-field calculation method and particularly estimate how the diffraction effects are taken into account by the FW-H formulation, a pure acoustic test case is proposed. The flap is removed and a pure monopole acoustics source (pressure and velocity time varying boundary conditions) positioned at the equivalent location. An acoustic LBM simulation is performed and the noise is recorded at the far-field microphones. The same numerical setup as the flow simulation is used.

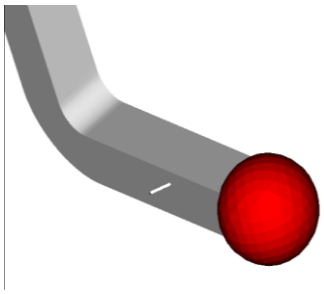

Figure 13. Measurement surface (red) used for porous FW-H formulation.

A snapshot of the instantaneous radiated pressure (Figure 14a) shows the acoustics waves produced by the monopole and radiating outside the duct toward the far-field microphones. From this acoustics simulation, a porous FW-H calculation is performed and the noise signals calculated at the 289 microphone locations. The comparison of the averaged SPL from the two methods is presented in Figure 14b. The results from the two approaches are in perfect agreement demonstrating that the noise can be accurately extrapolated from the porous surface to the far-field microphones.

The same method is applied using simulations B transient inputs recorded on the sampling surface. The averaged FW-H SPL results in Figure 15a are in very satisfying agreement with the experiments and the overall levels reduced by 5-7 dB compare to the directly simulated results. Figure 15b shows that the low frequency content

present in the LBM results at microphone D are removed from the FW-H calculation and compare better to the filtered measurements. Similarly to the experiments, peaks are visible in the FW-H results. It is assumed that they are also present in the LBM predictions but are masked by the contribution of the jet. One of the conclusions of this study is that considering that the microphones are not shielded with foam in LBM, the recorded pressure signals contain a significant contribution corresponding to the jet pseudo-noise. This contribution affects the low and high frequencies and comparisons to experiments have to be carefully analyzed particularly when low levels are involved For production cases, this importance is less significant. The same type of method has been applied on production defrost systems from automotive HVAC systems to suppress the pseudo-noise contribution from near-field microphones[33].

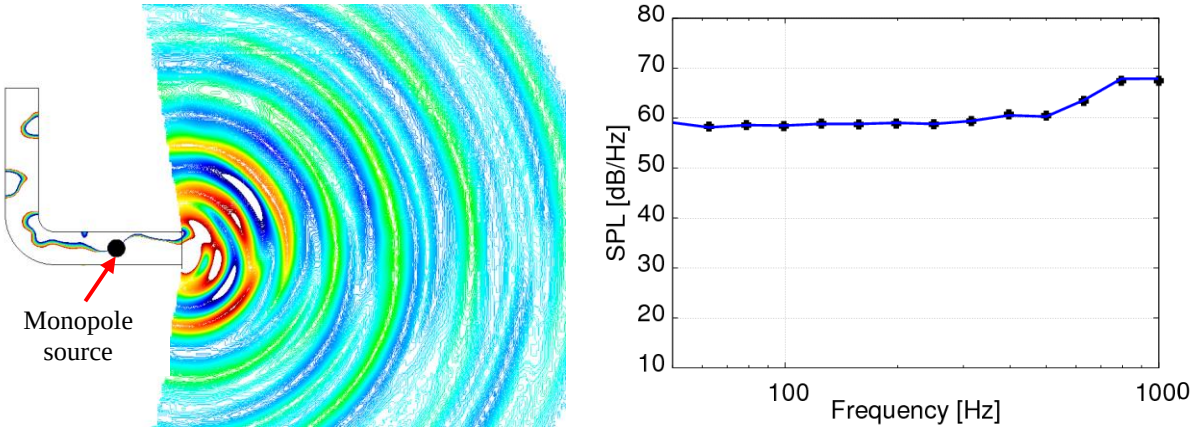

(a) (b)

Figure 14. (a) Instantaneous pressure field from monopole source inside the duct. (b) averaged SPL over 289 microphones: (——) Direct LBM; (● ●) LBM + FW-H.

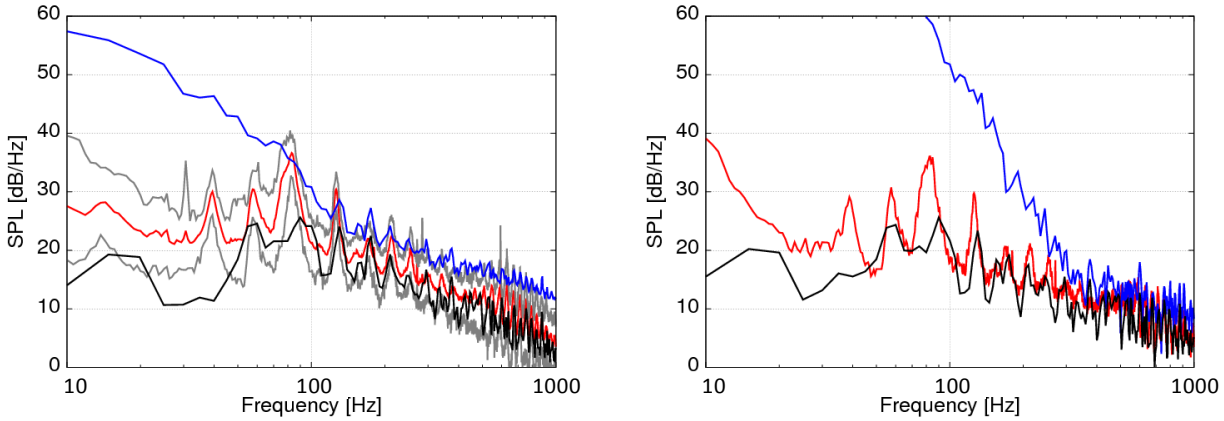

(a) (b)

Figure 15. Radiated noise: (a) averaged SPL; (b) microphone D; (——) experiments; (——) minimum and maximum experimental SPL; (——) LBM; (——) LBM + FW-H.

V. Conclusions

In this paper the flow and noise produced by a simplified HVAC elbow duct are discussed. Transient and compressible CFD/CAA simulations are carried out using a Lattice Boltzmann Method and compared to measurements. The flow and the radiated noise are predicted within the same calculations and no coupling between CFD information and acoustics solver is required. The predicted mean flow is compared to PIV measurements and the correct flow topology and strength is recovered in the simulations. The inlet profile is shown to influence the flow separation at the bend induced by an adverse pressure gradient. Another effect of the inlet profile is to modify the flow at the duct exit which can have an effect on the pressure fluctuations. The wall pressure fluctuations are accurately predicted in regions where the flow is fully separated implying that the transient simulations accurately capture the convected flow structures in the fluid. The turbulent flow activity is located downstream the flap certainly corresponding to the locations of the dominant flow-induced noise sources. In particular, a vortex shedding related to the presence of the flap is shown to significantly contribute to the tonal response of the system. Ongoing simulations performed at higher flow rates, not reported in this paper, show that the frequency of the peak at 80 Hz is shifted in frequency by the ratio of the mass flow rates. This is additional evidence that this mechanism is related to a vortex shedding-type activity. In quite areas, dominated by turbulent boundary layer fluctuations, the calculations do not capture the tiny near-wall structures explaining the underestimation of the levels in certain areas. For such a low Mach number configuration, the turbulent boundary noise is however known as a negligible source and this underestimation should not be affecting the radiated noise results. This hypothesis is confirmed with the far-field noise SPL showing satisfying comparisons between the simulations and the experiments and little influence of the inlet profile is observed. Using an acoustic analogy formulation, the pseudo-noise contribution is filtered out from the predicted SPL. The comparisons to the experiments, also filtered, are even better. This result demonstrates the possible importance of the pseudo noise contribution in the simulations and the ability of LBM at predicting duct noise.

References

[1] Pérot, F., Kim, M.S., Freed , D.M., Dongkon, L., Ih, K.D., Lee, M.H., 2010a, "Direct aeroacoustics prediction of ducts and vents noise", AIAA paper 2010-3724, 14th AIAA/CEAS aeroacoustics conference, Stockholm, June.

[2] K.D. Ih, S.R. Shin, S. Senthooran, B. Crouse and D.M. Freed, "Activities of Digital Wind Noise Testing Process for Virtual Prototype Development", 2009 JSAE Annual Congress, 203-20095476

[3] Pérot, F., Meskine, M., LeGoff, V., Vidal, V., Vergne, S., Dupuy, F., "Flow-induced noise predictions of complete HVAC systems using a Lattice Boltzmann Method", 7th international Symposium on Automotive and Railway comfort, Oct. 24-35, 2012 Le Mans, France

[4] Adam, J.L., Ricot, D., Dubief, F. and Guy, C. "Aeroacoustic Simulation of Automotive Ventilation Outlets", Proc. Acoustics 08 Conference., Paris, June 29, 2008.

[5] Pérot, F., Meskine, M., Gille, F., Sandrine, V. "Aeroacoustics prediction of simplified and production automotive HVAC ducts and registers", 15th AIAA/CEAS Aeroacoustics, AIAA-2011-2935, Stockholm, Sweden.

[6] Lee, D., Pérot, F., Ih, K.D. , Kim M.S., Freed, D.M., "Aeroacoustics predictions of automotive HVAC systems", 2010 SAE World Conference, April 2010

[7] Norisada K., Asano H., Kitada M., Hirayama S., Ishii T., Sasaki N., Pérot, F., Wada K., "Prediction of Aero-acoustic Noises from an Automotive HVAC", Japan CFD symposium, December 2010

[8] Pérot, F., Wada, K., Norisada, K., Kitada, M., Hirayama, S., Sakai, M., Imahigasi, S., Sasaki, N., "HVAC Blower Aeroacoustics Predictions Based on the Lattice Boltzmann Method", AJK2011-23018, AJK Conference, Hamamatsu, Japan.

[9] Norisada, K., Sakai, M., Ishiguro, S., Kawaguchi, M., Pérot, F., Wada K.," HVAC Blower Aeroacoustic Predictions", 2013 SAE World Congress, April 2013

[10] Lee, D., Pérot, F., Freed , D.M., Ih, K.D., "Prediction of Flow Induced Noise Related to Automotive HVAC Systems", 2011 SAE World Congress and Exhibition, paper 2010-0493, April 2011.

[11] Jäger, A., Decker, D., Hartmann, M., Islam, M., Lemke, T., Ocker, J., Schwarz, V., Ullrich, F., Crouse B., Balasubramanian, G., Mendonca, F. and Drobietz, R., "Numerical and Experimental Investigations of the Noise Generated by a Flap in a Simplified HVAC Duct", 14th AIAA/CEAS Aeroacoustics Conference, AIAA2008-2902

[12] Brès, G.A., Pérot, F., Freed, D. "Properties of the Lattice-Boltzmann Method for Acoustics", AIAA 2009-3395, 13th AIAA/CEAS aeroacoustics conference, Miami, Florida, 2009
[13] Laffite, A., Pérot, F., "Investigation of the Noise Generated by Cylinder Flows Using a Direct Lattice-Boltzmann Approach", AIAA 2009-3268, 13th AIAA/CEAS aeroacoustics conference, Miami, Florida, 2009
[14] Martínez-Lera, P., Hallez, R., Tournour, M., Schram, C., Improved simulation technique for predicting the noise radiated by a flap in a simplified HVAC duct", 2011, JSAE Annual Congress, 20115259
[15] Carton de Wiart, C., Philippe Geuzaine, P., Detandt , Y., Manera, J., Caro, S., Marichal, Y., Winckelmans, G., "Validation of a Hybrid CAA Method: Noise Generated by a Flap in a Simplified HVAC Duct", 19th AIAA/CEAS aeroacoustics conference, AIAA2010-3995
[16] Pérot, F., Meskine, M., and Vergne S., 2009, "Investigation of the Statistical Properties of Pressure Loadings on Real Automotive Side Glasses", AIAA paper 2009-3402, 13th AIAA/CEAS aeroacoustics conference, Miami, Florida.
[17] Senthooran, S., Crouse, B., Balasubramanian, G., Freed, D., Shin S.R., and Ih, K.D., "Effect of Surface Mounted Microphones on Automobile Side Glass Pressure Fluctuations", Proc. 7th MIRA Intl. Vehicle Aerodynamics Conf., Richoh Arena, UK, Oct.22, 2008.
[18] Crouse, B., Balasubramanian, G., Senthooran, S., Freed, D., Ih, K.D. and Shin, S.R., "Investigation of Gap Deflector Efficiency for Reduction of Sunroof Buffeting', SAE conference 2009-01-2233, 2009
[19] Pérot, F., Freed, D., "Acoustic absorption of porous materials using LBM", 19th AIAA/CEAS Aeroacoustics conference, Berlin, Germany, 2013
[20] Mann, A., Pérot, F., Kim, M.S., Casalino, D., "Characterization of Acoustic Liners Absorption using a Lattice-Boltzmann Method", 19th AIAA/CEAS Aeroacoustics conference, Berlin, Germany, 2013
[21] Pérot, F., Moreau, S., Henner, M., Neal, D. and Kim, M. "Direct Aeroacoustic Prediction of a Low-Speed Axial Fan", AIAA paper 2010-3887, 2010.
[22] Pérot, F., Kim, M., Le Goff, V., Carniel, X., Goth, Y., Chassaignon, C., "Numerical Optimization of the Tonal Noise of a Centrifugal Fan Using a Flow Obstruction", Fan2012 International Conference, April 2012, Senlis, France.
[23] Mann, A., Pérot, F., Kim, M.S. Casalino, D., Fares, E,.(2012), " Advanced Noise Control Fan Direct Aeroacoustics Predictions using a Lattice-Boltzmann Method", 18th AIAA/CEAS Aeroacoustics conference, AIAA2012-2287, Colorado Springs, CO, USA
[24] Casalino, D., Noelting, S., Fares, E., Van de Ven, T., Pérot, F., G.A. Brès, " Towards Numerical Aircraft Noise Certification: Analysis of a Full-Scale Landing Gear in Fly-Over Configuration", AIAA2012-2235, Colorado Springs, CO, USA
[25] Bhatnagar, P., Gross, E., Krook, M., "A model for collision processes in gases. I. small amplitude processes in charged and neutral one-component system", Pys. Rev., vol.94, pp.511-525, 1984.
[26] Shan, X. and Chen, H., "Lattice Boltzmann model for simulating flows with multiple phases and components", Phys. Rev. E, 47, 1815-1819, 1983.
[27] Chen, H., Orszag, S., Staroselsky, I., Succi, S. "Expanded Analogy between Boltzmann Kinetic Theory of Fluid and Turbulence", J. Fluid Mech., Vol. 519, pp. 301-314, 2004.
[28] Chen, H., Teixeira, C., Molvig, K., "Realization of Fluid Boundary Conditions via Discrete Boltzmann Dynamics," Intl J. Mod. Phys. C, Vol. 9 (8), pp. 1281-1292, 1998.
[29] Chen, H., "Volumetric Formulation of the Lattice Boltzmann Method for Fluid Dynamics: Basic Concept", Phys. Rev. E, Vol. 58, pp. 3955-3963, 1998.
[30] Brès, G.A., Freed, D., Wessels, M., Noelting, S., Pérot, F., "Flow and noise predictions for the tandem cylinder aeroacoustic benchmark", Phys. Fluids 24, 036101 (2012); doi: 10.1063/1.3685102
[31] Meskine, M., Pérot, F., Kim, M.S, Senthooran, S., Freed, D.M, Sugiyama, Z., Gautier, S., " High speed train aeroacoustic solution for community and interior noise using Lattice Boltzmann Method", 7th Automotive and Railroad Comfort Symposium, SIA 2012, Le Mans, France
[32] Meskine, M., Pérot, F., Kim, M.S, Senthooran, S., Freed, D.M, Sugiyama, Z., Gautier, S., "Community noise prediction of digital high speed train using LBM", 19th AIAA/CEAS Aeroacoustics Conference, May 2013, Berlin, Germany.
[33] Pérot, F., Meskine, M., Vergne, S., "HVAC noise predictions using a Lattice Boltzmann Method", 19th AIAA/CEAS Aeroacoustics conference, May 2013, Berlin, Germany, 2013